

Synthesis of Mg Alkoxide Nanowires from Mg Alkoxide Nanoparticles upon Ligand Exchange

Shunrui Luo, Kostiantyn Turcheniuk, Lihua Chen, Ah-Young Song, Wenqiang Hu, Xiaolei Ren, Zifei Sun, Rampi Ramprasad, and Gleb Yushin*



Cite This: *ACS Appl. Mater. Interfaces* 2022, 14, 13820–13827



Read Online

ACCESS |



Metrics & More



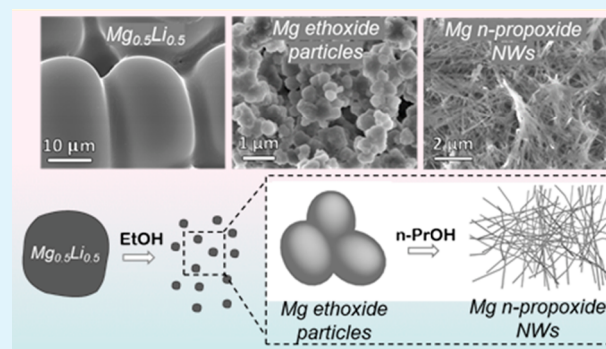
Article Recommendations



Supporting Information

ABSTRACT: We report on a new synthesis pathway for Mg *n*-propoxide nanowires (NWs) from Mg ethoxide nanoparticles using a simple alkoxy ligand exchange reaction followed by condensation polymerization in *n*-propanol. In order to uncover the morphology–structure correlation in the metal alkoxide family, we employed a powerful range of state-of-the-art characterization techniques. The morphology transformation from nanoparticles to nanowires was demonstrated by time-lapse SEM micrographs. Fourier transform infrared spectroscopy (FTIR) and nuclear magnetic resonance spectroscopy (such as ^1H NMR and solid-state ^{13}C cross-polarization (CP)-MAS NMR) illustrated the replacement of ethyl by *n*-propyl and metal alkoxide condensation polymerization. We identified chemical formulas of the products also using NMR spectroscopy. The crystal structure simulation of Mg ethoxide particles and Mg *n*-propoxide NWs provided insights on how the ligand exchange and the associated increase in the fraction of OH groups greatly enhanced Mg alkoxide bonding and enabled a higher degree of coordination polymerization to facilitate the formation and growth of the Mg *n*-propoxide NWs. The discovered synthesis method could be extended for the fabrication of other metal alkoxide (nano) structures with various morphologies.

KEYWORDS: Mg alkoxides, nanowires, ligand exchange, morphology–structure correlation, growth mechanism



INTRODUCTION

The versatile ancillary ligands, highly varied steric structure, and diverse metal ions allow metal alkoxides and their derivatives to offer high solubility in many organic solvents and a broad range of chemical and physical properties for multiple industrial applications.^{1–3} Metal alkoxides are also highly reactive and often rapidly undergo hydrolysis (reaction with water, if present), alcoholysis (reaction with other alcohols), condensation (combining smaller molecules into larger ones), and gelation (forming three-dimensional networks) to form alkoxide oligomers and polymers. They are often used as catalysts or intermediates in polymerization, trans-esterifications, and condensations⁴ and as precursors for the formation of oxides in the form of the bulk ceramics or nanostructured materials and thin films,^{5–7} often using chemical vapor deposition (CVD) techniques.

Recently, we reported a new mechanism for the formation of alkoxide nanowires (NWs), which was based on the strain energy minimization at the boundary of the chemical transformation front and enabled direct transformation of bulk bimetallic Al–Li and Mg–Li alloys into Al alkoxide NWs upon the alloys' exposure to suitable alcohols.^{8–10} In the case of Mg alkoxide (propoxide) NWs, the suitable alcohols were found to be *n*-propanol or iso-propanol, while ethanol was

found to produce Mg ethoxide particles.¹⁰ In the prior art studies, ligand exchange has been applied for the preparation of nanostructures with specific morphology through colloidal syntheses.¹¹ For example, when mixing a solution of HAuCl_4 with hexadecyltrimethylammonium bromide (CTAB) at a concentration above its critical micelle concentration, the ligand exchange between the counterion (Br^-) of CTAB and the counterion (Cl^-) of HAuCl_4 resulted in the formation of CTAB micelles, which enabled the formation of Au 1D nanostructures.^{12,13} In one recent example, ZIF-8 nanocrystals/Au nanobelts were prepared by replacing benzenedicarboxylate in ZnBDC nanoplates with oleylamine in the presence of HAuCl_4 .¹⁴ The morphological change was quite significant, although the shape change mechanism was not studied in detail.

Here we report on another interesting phenomenon, where alkoxy ligand exchange of freshly produced Mg ethoxide

Received: November 15, 2021

Accepted: March 2, 2022

Published: March 14, 2022



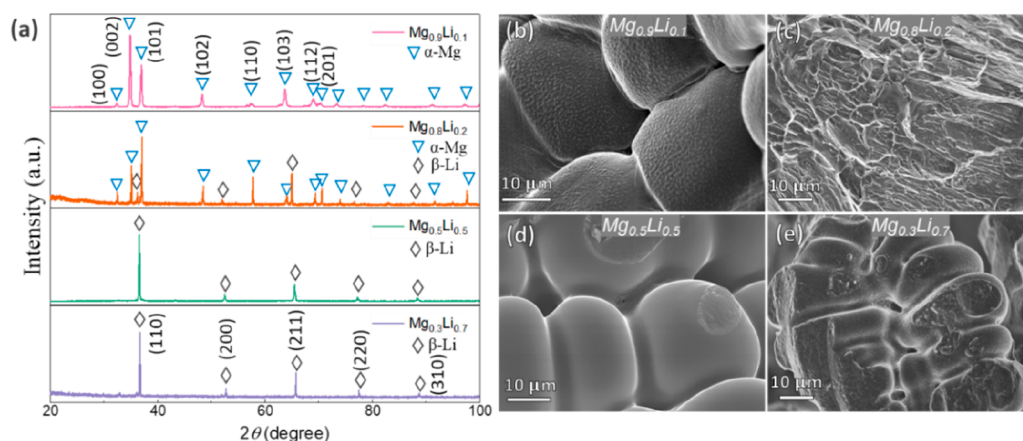


Figure 1. XRD pattern (a) and scanning electron microscopy (SEM) (b–e) micrographs of $\text{Mg}_{0.9}\text{Li}_{0.1}$, $\text{Mg}_{0.8}\text{Li}_{0.2}$, $\text{Mg}_{0.5}\text{Li}_{0.5}$, and $\text{Mg}_{0.3}\text{Li}_{0.7}$.

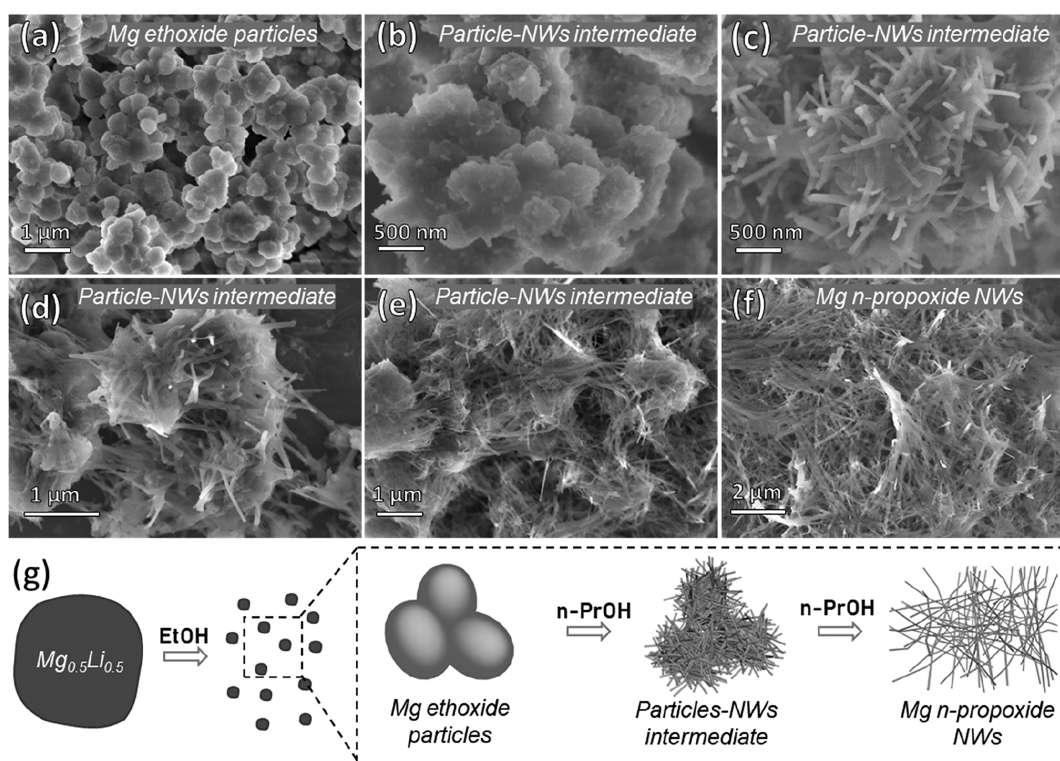


Figure 2. Time-lapse micrographs of swelling (a) Mg ethoxide-50 particles in *n*-propanol for 1 h (b), 6 h (c), 12 h (d), 36 h (e), and 72 h (f) at 80 °C. (g) Schematic illustration of the transformation of $\text{Mg}_{0.5}\text{Li}_{0.5}$ to Mg *n*-propoxide NWs.

particles or nanoparticles (NPs) upon their exposure to *n*-propoxide leads to the condensation polymerization and the formation of Mg *n*-propoxide NWs. To our knowledge, this is the first time such a dramatic morphological change (from nanoparticles to NWs) has been reported through simple alcohol ligand exchange (i.e., alcohol interchange reaction). Crystal simulations provided additional insights on the configuration of Mg *n*-propoxide NWs and Mg ethoxide NPs, helping us to reveal the NW growth mechanism. The diameters of the NWs were found to be tunable by the shape, size, porosity, and ligand group of Mg alkoxide precursors. The obtained Mg alkoxides could be further used for catalysis,^{15,16} energy conversion and storage,¹⁷ and high-tech metal oxide nanomaterials^{18–20} among other applications.

RESULTS AND DISCUSSION

Synthesis of MgLi Alloys as Precursors for Ethoxide Nanoparticles. $\text{Mg}_x\text{Li}_{1-x}$ alloys, in which $x = 0.1, 0.2, 0.5,$ and 0.7 , were prepared by a rapid heating process of the mixtures of Mg and Li metals. X-ray diffraction (XRD) analysis of the alloys shows the presence of crystalline Mg–Li phases without noticeable metal oxide or metal carbide impurities (Figure 1). Also, no slags were observed when the obtained alloys were cut into small pieces. The $\text{Mg}_{0.9}\text{Li}_{0.1}$ alloy consists of only an α -Mg phase, which confirms the homogeneity of the prepared sample (Figure 1a). Scanning electron microscopy (SEM) shows the average diameter of the alloy grain of 30–40 μm with well-defined elongated geometry. The binary $\text{Mg}_{0.8}\text{Li}_{0.2}$ alloy consists of a dual α -Mg phase and β -Li phase.²¹ A good agreement of the position of $\text{Mg}_{0.8}\text{Li}_{0.2}$ alloy XRD peaks with

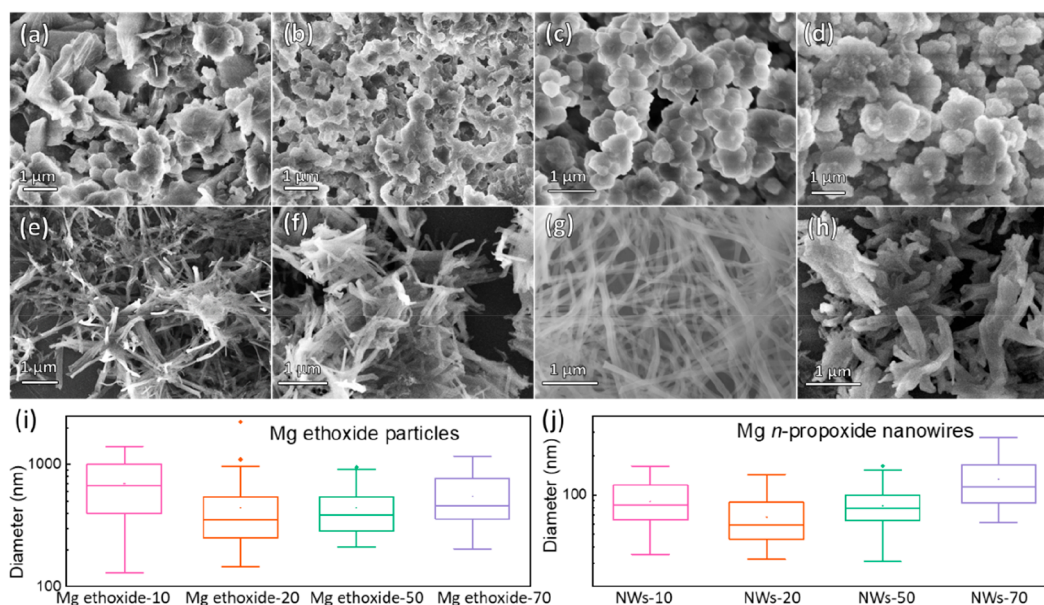


Figure 3. SEM micrographs of (a) Mg ethoxide-10, (b) Mg ethoxide-20, (c) Mg ethoxide-50, and (d) Mg ethoxide-70 dealloyed from $\text{Mg}_{0.9}\text{Li}_{0.1}$, $\text{Mg}_{0.8}\text{Li}_{0.2}$, $\text{Mg}_{0.5}\text{Li}_{0.5}$, and $\text{Mg}_{0.3}\text{Li}_{0.7}$ alloy with ethanol, respectively. Mg *n*-propoxide NWS: (e) NWS-10, (f) NWS-20, (g) NWS-50, and (h) NWS-70 obtained from swelling Mg ethoxide-10, Mg ethoxide-20, Mg ethoxide-50, and Mg ethoxide-70 in *n*-propanol at 80 °C for 3 days, respectively. (i, j) Diameter and width distribution of Mg ethoxide particles and Mg *n*-propoxide nanowires.

$\text{Li}_{0.184}\text{Mg}_{0.816}$ (ICDD Card No. 04-003-6264) was observed. Rod-like alloy grains were observed in $\text{Mg}_{0.8}\text{Li}_{0.2}$ alloy, which is commonly found in eutectic alloys (Figure 1c). The elements of Mg and O (which indicates the position of Li) were distributed homogeneously according to the EDS results (Figure S1). The $\text{Mg}_{0.5}\text{Li}_{0.5}$ and $\text{Mg}_{0.3}\text{Li}_{0.7}$ alloys are both composed of only a β -Li phase, indicating the homogeneity of the synthesized phases. The $\text{Mg}_{0.5}\text{Li}_{0.5}$ alloy appears in the largest grain size (40–60 μm) among the synthesized samples with well-defined grain boundaries. The darker contrast of the grain boundaries indicates their Li-rich nature as compared to the alloy grains, which could facilitate the reaction with alcohols. The $\text{Mg}_{0.3}\text{Li}_{0.7}$ alloy appears in the form of elongated egg-shaped grains with well-defined grain boundaries. The absence of the differences in contrast allows one to assume that the composition of the grain boundaries and alloy is homogeneous (Figure S1). MgLi alloy with a higher Li content would result in a higher reactivity (e.g., with alcohols).⁸

Dealloying of MgLi Alloys in Ethanol to Form Mg Ethoxide Nanoparticles. The dissolution of Li from the MgLi alloys creates the conditions for residual Mg (not protected by the surface native oxide film) to react with alcohols with the formation of insoluble alkoxide species (the involved chemical reaction is $\text{MgLi} + \text{EtOH} \rightarrow \text{LiOEt} + \text{Mg}(\text{OEt})_2 + \text{H}_2\uparrow$), while LiOEt could be easily removed due to its high solubility in ethanol. In the case of *n*- or isopropanol, gradually produced Mg propoxides exhibit 1D (NW) morphology.^{8,10} However, much faster room temperature dealloying of the MgLi alloys in ethanol resulted in the formation of white precipitates—spherical agglomerates of NPs with an average diameter of 2–3 μm—as was evidenced by the SEM analysis.^{1,3} The observed difference in the reaction rate and/or the chemical composition of the alkoxide species may play a major role in the shape-control over the Mg alkoxides and favor formation of either 1D structures (in propanol) or small particles (in ethanol).

Ligand Exchange in Mg Ethoxide Particles. In this study, we want to test a hypothesis that the chemistry of the ligand (propoxide vs. ethoxide) may have a significant impact on either the tendency or the ability of the Mg alkoxide to form NWS. To investigate such an impact, we deployed the alkoxide exchange strategy by initially forming the Mg ethoxide particles and then replacing the ethoxide ligands by the *n*-propoxide ligands (the main chemical reaction is $\text{Mg}(\text{OEt})_2 + n\text{-PrOH} \rightarrow \text{Mg}(\text{OEt})_2 + \text{EtOH}$). For this, we reacted freshly formed Mg ethoxide nanoparticles with *n*-propanol at 80 °C for 72 h. The choice of the propanol solvent and reaction conditions was based on our previous findings of the one-step NW formation upon exposure of MgLi to propanol alcohols.¹⁰ The mechanism of alcohol interchange reaction is a well-known bimolecular nucleophilic substitution reaction ($\text{S}_{\text{N}}2$), where Mg ethoxide molecules bind *n*-PrOH (attacking nucleophile) to give a discrete intermediate, followed by a fast loss of $-\text{OEt}$ ligand.²² To our surprise, the ligand exchange in all four studied samples resulted in the appearance of NWS, as revealed by the SEM analyses (Figures 2 and 3).

NW Growth Mechanism. Figure 2 shows the evolution of NWS from bulk particles at different time intervals. The starting point of the reaction denotes the aggregates of irregular spheroidal nanoparticles with an average diameter of ~400 nm and moderate surface roughness (Figure 2b). After 1 h at 80 °C, the surface of Mg ethoxide evolved into a protruded surface with 10–20 nm bumps in diameter (Figure 2c). At 6 h of reaction time, we observed the formation of the axially oriented NWS that grew axially from the particle surface. The NWS exhibit an average length ranging 500 nm and an average diameter of ~50 nm (Figure 2c). Upon further Mg ethoxide-to-Mg *n*-propoxide transformation, these NWS continue to grow from the particle surface without noticeable orientation. Between 12 and 36 h of reaction time, the surface of the particles noticeably erodes (Figure 2e), rendering their complete consumption after 72 h. A full-grown NW is ~5 μm

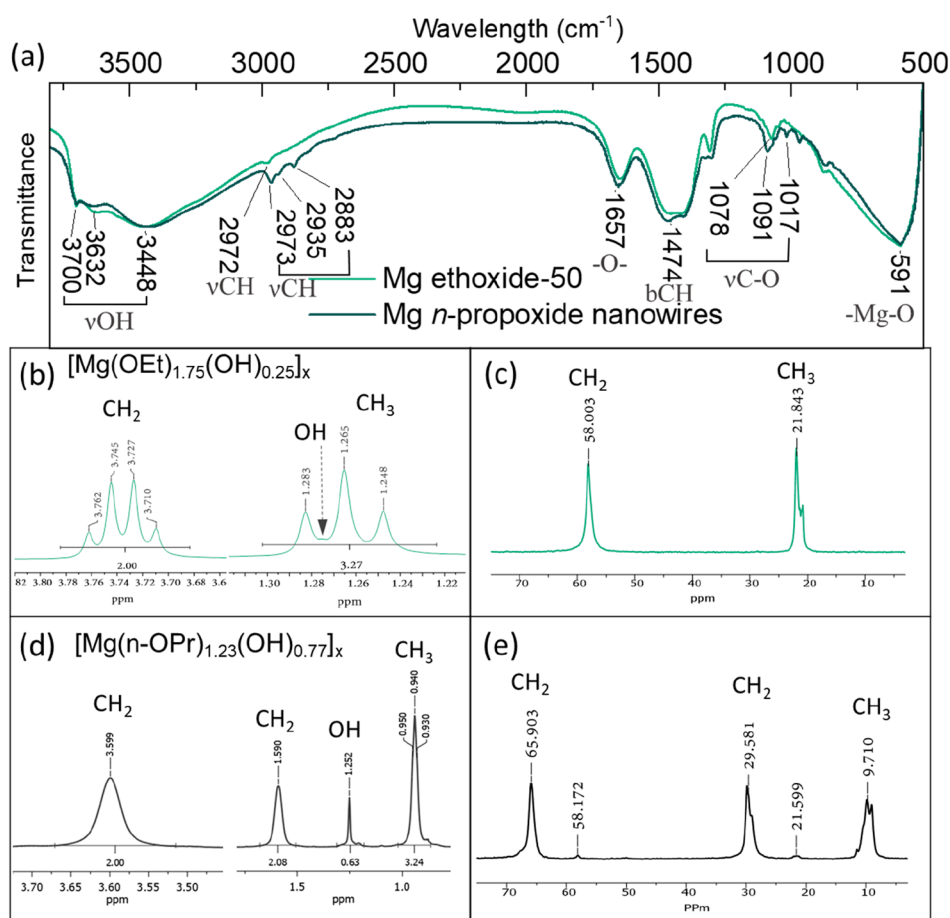


Figure 4. (a) FTIR spectrum of Mg ethoxide and Mg *n*-propoxide nanowires. Abbreviations: ν - stretching, b - bending. (b, d) Solution ¹H NMR of the Mg ethoxide-50 particles and Mg *n*-propoxide NWs, respectively. Chemical shifts in solution NMR are relative to internal TMS ($d=0$). (c, e) Solid state ¹³C cross-polarization (CP) magic-angle-spinning (MAS) NMR spectra of the Mg ethoxide-50 particles and Mg *n*-propoxide NWs, respectively. Chemical shifts are relative to internal TMS ($d = 0$). The ¹³C chemical shifts in solid-state NMR are calibrated with respect to the adamantane at 38.45 ppm.

in length, while retaining ~ 80 nm diameter and exhibiting an aspect ratio of ~ 60 .

Condensation of Mg *n*-propoxide ($\text{OPr}^n\text{-Mg-OPr}^n + \text{OPr}^n\text{-Mg-OPr}^n \rightarrow \text{OPr}^n\text{-Mg-O-OPr}^n + \text{Pr}^n\text{OPr}^n$) takes place, accompanying the ligand exchange reaction. The newly formed Mg *n*-propoxide oligomer complexes aggregate as nuclei attach to the surface of Mg ethoxide particles. Note that the transformation from the Mg ethoxide to Mg *n*-propoxide should be accompanied by a substantial volume increase ($\sim 30.6\%$ based on the molecular volume of $\text{Mg}(\text{OEt})_2$ and $\text{Mg}(\text{OPr}^n)_2$) because *n*-propoxide ligands are bulkier (compare $-\text{C}_2\text{H}_5\text{OH}$ with $-\text{CH}_3\text{CH}_2\text{CH}_2\text{OH}$). The volume expansion will be accompanying the overall process, inducing stresses at the boundary of the Mg ethoxide/Mg *n*-propoxide interphase. The nanowire morphology minimizes such interface stress energy. The diameter of the Mg *n*-propoxide NWs may be affected by the interplay between lowering the total NW interfacial strain energy (smaller diameter NWs should lead to smaller NW strain energy) and lowering the total NW surface energy (larger diameter NWs should lead to smaller NW surface energy). The 1D shape of the *n*-propoxide species may also be related to the detected presence of the hydroxyl ($-\text{OH}$) groups, which facilitate H-bonding and directional (1D) growth, as will be discussed below.

Tunable Nanowires Synthesized from Other Mg Alkoxide Precursors.

We found that the dimensions of the Mg *n*-propoxide NWs depend on the size and morphology of the Mg ethoxide particles, which, in turn, are somewhat controlled by the MgLi alloy composition. As an example, Figure 3 shows a difference in the morphology and size of Mg ethoxide obtained from the reaction with MgLi alloys having different Li content. Mg ethoxide-10 (obtained from $\text{Mg}_{0.9}\text{Li}_{0.1}$) shows a morphology of dense fragmented particles (~ 700 nm, Figure 3a). The Mg *n*-propoxide NWs obtained by the ligand exchange with Mg ethoxide-10 exhibit an average diameter of ~ 90 nm and feature connected ends, as may be expected from their formation from the individual dense ethoxide particles (Figure 3d). The analysis of BET nitrogen adsorption-desorption isotherms shows the lowest BET specific surface area (SSA) for Mg ethoxide-10 of all four studied homemade Mg ethoxides (Figure S2a). The limited pores in Mg ethoxide-10 may impede the diffusion of *n*-propanol molecules and further result in extended time for full ligand exchange reaction. The Mg ethoxide-20 particles are the smallest of all studied ethoxide particles with nanoparticles ~ 150 nm linked together into larger (porous) aggregates (Figure 3b). Their larger BET SSA is indicative of much higher pore volume (Figure S2a), which could enable a fast and uniform alkoxy ligand exchange. The NWs yielded from the

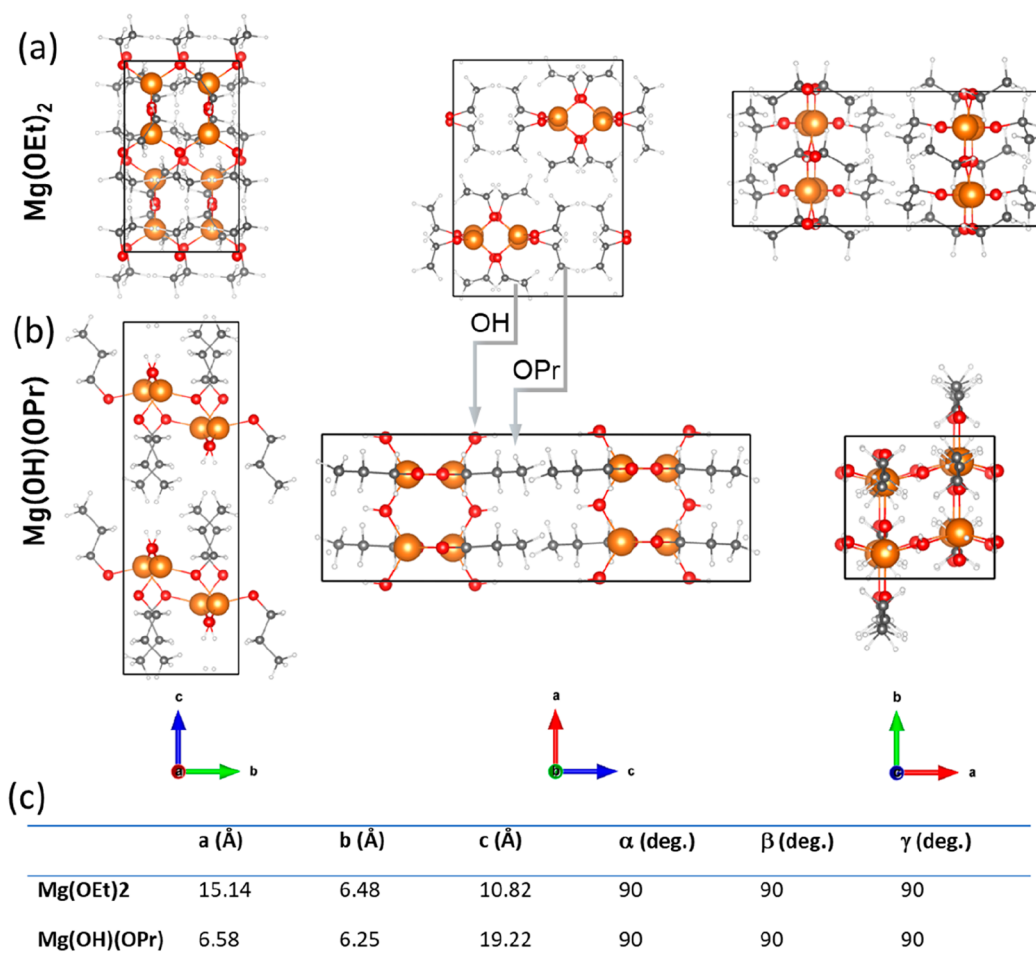


Figure 5. Crystal structures of (a) Mg ethoxide and (b) Mg *n*-propoxide. Mg, C, H, and O atoms are denoted by orange, gray, white, and red spheres. (c) Geometric parameters of crystal structures of Mg ethoxide and Mg *n*-propoxide.

Mg ethoxide-20 exhibit an average diameter of ~ 65 nm with a relatively narrow distribution (Figure S2e,g) and dense packing (bundling). The latter could be explained by the volumetric expansion of the Mg *n*-propoxide NWs over Mg ethoxide particles. The Mg ethoxide-70 particles exhibit a nonuniform particle diameter from 20 nm to 1 μm yielding NWs with an average diameter of ~ 130 nm. The DFT pore size distribution plots of Mg ethoxide-70 and Mg ethoxide-50 are similar, while Mg ethoxide-70 exhibits a higher BET SSA and higher mesoporous pore volume, which would shorten the required time for full ligand exchange reaction. We speculate the local high concentration of Mg *n*-propoxide monomer (or oligomer) helps in the formation of NWs with a wide width.

Comparative Structural and Spectral Analysis of Mg Ethoxide Particles and Mg *n*-Propoxide NWs. In FT-IR, stronger aliphatic C–H stretching absorption was observed in NWs as compared to precursor ethoxide particles (Figure 4a). This suggests successful ligand replacement, since the C–H aliphatic signals are expected to be more pronounced in the *n*-propyl group.^{23,24} Both samples feature strong vibrational OH peaks, indicating the contribution of OH groups to NWs and particle bonding. The OH may possibly be originated from the partial hydrolysis or thermolysis of magnesium alkoxides (Mg(OEt)₂ and Mg(*n*-OPr)₂) to polymeric metal oxoalkoxides (Mg–O chain surrounded by OR groups).²⁵ The presence of vibrations at 3700 and 3632 cm^{-1} suggests the contribution of

H-bondings (O \cdots H–O– bondings and bridging O–H–groups).²⁴ We assigned the high wavenumber peak at 1657 cm^{-1} to bridging hydroxy (–O–H) or oxy groups (–O–R), which was usually found in magnesium ethanoate and methanolate and caused by their aggregation.^{24,26}

¹H NMR (nuclear magnetic resonance) and ¹³C NMR spectra of NWs demonstrate almost a complete alkoxide exchange featuring only small residual peaks of ethoxy groups at 21.599 and 58.172 ppm in solid-state ¹³C NMR (Figure 4e). The integration of the peaks gives the [Mg(OH)_{0.25}(OEt)_{1.75}] and [Mg(OH)_{0.77}(*n*-OPr)_{1.23}] chemical formula for Mg ethoxide particles and Mg *n*-propoxide NWs, respectively, shows consistency with the FTIR (Figure 4a) and TGA data (Figure S4). In this regard, due to the detected partial hydrolysis or thermolysis of the alkoxides, the NWs may also be called hydroxy-propoxide NWs. Interestingly, the NWs feature a much higher (~ 3 times) content of OH groups as compared to the parent particles. This could be due to the larger steric hindrance of *n*-propoxy groups, which allows larger accommodation of small OH groups. We would like to emphasize that this larger presence of OH groups could lead to the presence of abundant sites for H-bonding to both strengthen the material and also achieve a higher degree of coordination polymerization, which is typical for metal organic alkoxides.²⁷ As such, these OH groups may enable the Mg *n*-propoxide NW growth upon the transformation of the parent

particles' surface $\text{Mg}(\text{OH})_{0.25}(\text{OEt})_{1.75}$ to final $\text{Mg}(\text{OH})_{0.77}(\text{n-OPr})_{1.23}$.

Steric Configuration Simulation. We used the USPEX evolutionary algorithm in order to reveal the bonding in the synthesized NWs and compare it to that in the regularly arranged $\text{Mg}(\text{OEt})_2$ particles. We found that both $\text{Mg}(\text{OEt})_2$ and $\text{Mg}(\text{OH})(\text{OPr})$ exhibit stable structures with 8 formula units per conventional cell (Figure 5c). We note that the Mg atoms in both $\text{Mg}(\text{OEt})_2$ and $\text{Mg}(\text{OH})(\text{OPr})$ have a coordination number of 4, as each Mg atom locates at the center of a regular tetrahedron formed by 4 oxygen atoms. However, Figure 5a shows that strong ionic bond connections between $\text{Mg}(\text{OEt})_2$ groups only extend along the *b* direction, while $\text{Mg}(\text{OEt})_2$ groups are held together at the other two directions by weak van der Waals forces. As a result, it is relatively easy to break $\text{Mg}(\text{OEt})_2$ groups if substantial internal stresses are present (resulting, e.g., from surface layer volume expansion upon the reaction of MgLi particles with ethanol), which may lead to $\text{Mg}(\text{OEt})_2$ pulverization and the formation of individual $\text{Mg}(\text{OEt})_2$ particles. In the case of $\text{Mg}(\text{OH})(\text{OPr})$, the small OH groups provide another bridge between Mg atoms, resulting in a 2-D plane with strong ionic bond connections, which enables $\text{Mg}(\text{OH})(\text{OPr})$ to withstand internal stresses and enables the formation and growth of 1D (NW) structures. From Figure 5, we note that $\text{Mg}(\text{OH})(\text{OPr})$ can be formed by replacing the $-\text{OEt}$ groups along the *a* and *c* directions with OH and OPr groups. The direction with OH groups can extend additional $-\text{Mg}-\text{OH}-\text{Mg}-\text{OH}$ bond connections. The calculated FTIR pattern based on the crystal structure of $\text{Mg}(\text{OH})(\text{OPr})$ NWs generated in USPEX shows a good match with the experimental FTIR peaks (Figure S5).

CONCLUSION

In this work, we reported for the first time a new catalyst-free and template-free fabrication of metalorganic nanowires (NWs) involving a simple alkoxy ligand exchange in spheroidal or irregularly shaped alkoxide particles. Here, Mg *n*-propoxide NWs have been produced from swelling Mg ethoxide particles in *n*-propanol at 80 °C and atmospheric pressure. The compositions of Mg ethoxide particles and Mg *n*-propoxide NWs were confirmed by FTIR and NMR analyses. All Mg alkoxide samples comprised some fractions of the OH groups, but their amounts in Mg *n*-propoxide NWs were significantly larger. The SEM micrographs recorded at different reaction intervals showed the gradual transformation of Mg ethoxide particles to Mg *n*-propoxide NWs. Crystal structure simulation of Mg ethoxide particles and Mg *n*-propoxide NWs demonstrated a significant difference in the bonding. The $\text{Mg}(\text{OEt})_2$ groups are held together by weak van der Waals forces, making Mg ethoxide rather weakly bonded and brittle and likely subject to pulverization into (nano)particles upon formation from the MgLi alloy due to volume-change-induced stresses. However, exposure of Mg ethoxide into *n*-propoxide at elevated temperature to induce the ligand exchange and increase the fraction of OH groups greatly enhanced Mg alkoxide bonding, which should not only improve alkoxide mechanical properties but also enable a higher degree of coordination polymerization to facilitate the formation and growth of the Mg *n*-propoxide NWs. We expect the discovered method to be applicable for the fabrication of other dense or porous metal alkoxide, metal hydroxy-alkoxide, and metal oxide nanostructures, including NWs.

EXPERIMENTAL SECTION

Chemicals. Lithium foil (battery grade, 0.75 mm, Sigma-Aldrich), magnesium chips (99.98% pure, 6–35 mesh Sigma-Aldrich), ethyl alcohol (pure, 200 proof, anhydrous, ≥99.5%, Sigma-Aldrich), *n*-propanol (pure, anhydrous, 99.7%, Sigma-Aldrich), *iso*-propanol (anhydrous, ≥99.5%, Sigma-Aldrich), methanol (pure, anhydrous, 99.9%, Alfa Aesar).

Synthesis of Mg–Li Alloys. MgLi alloys with various Li contents (10, 20, 50, and 70 at. % of Li, marked as $\text{Mg}_{0.9}\text{Li}_{0.1}$, $\text{Mg}_{0.8}\text{Li}_{0.2}$, $\text{Mg}_{0.5}\text{Li}_{0.5}$, and $\text{Mg}_{0.3}\text{Li}_{0.7}$, respectively) were prepared via the method reported by us previously.^{8,10} Typically, 243.05 g of Mg and 69.41 g of Li were used to produce $\text{Mg}_{0.5}\text{Li}_{0.5}$ alloy. The Mg chips and Li strips were mixed and then heated rapidly to 750 °C (~500 °C for $\text{Mg}_{0.3}\text{Li}_{0.7}$ alloy preparation) at a heating rate of ~895 °C min⁻¹ in a graphite crucible with an induction heater (Fluxcon Roy1500, USA). The temperature and heating rate were measured by an optical pyrometer (Calex PyroUSB 2.2, USA). The heating was stopped once the temperature reached ~750 °C. The crucible was shaken a couple of times for better mixing, and then, the solution phase mixture was quenched into another graphite crucible. The alloy pellet was collected after being cooled to room temperature. $\text{Mg}_{0.9}\text{Li}_{0.1}$ alloy (218.74 g of Mg and 6.94 g of Li), $\text{Mg}_{0.8}\text{Li}_{0.2}$ alloy (213.88 g of Mg and 15.27 g of Li), and $\text{Mg}_{0.3}\text{Li}_{0.7}$ alloy (145.83 g of Mg and 97.17 g of Li) were prepared though the same process.

Dealloying Reaction. In a typical dealloying process, an alloy pellet was immersed in 20 mL of anhydrous ethanol. When the alloy pellet was fully reacted, white precipitate was collected and washed with ethanol three times and then dried at ambient pressure under an inert atmosphere. Mg ethoxide-10, Mg ethoxide-20, Mg ethoxide-50, and Mg ethoxide-70 particles were obtained though dealloying $\text{Mg}_{0.9}\text{Li}_{0.1}$, $\text{Mg}_{0.8}\text{Li}_{0.2}$, $\text{Mg}_{0.5}\text{Li}_{0.5}$, and $\text{Mg}_{0.3}\text{Li}_{0.7}$ alloy with ethanol at room temperature, respectively.

Mg *n*-propoxide nanowires (NWs-50) were prepared through swelling Mg ethoxide (Mg ethoxide-50) in anhydrous *n*-propanol at 80 °C at an elevated time. Then, Mg *n*-propoxide nanowires were separated via centrifugation and dried at ambient pressure under an inert atmosphere for further use. Mg *n*-propoxide nanowires obtained after the same process from Mg ethoxide-10, Mg ethoxide-20, and Mg ethoxide-70 are marked as NWs-10, NWs-20, and NWs-70, respectively.

Materials Characterization. Scanning electron microscopy (SEM) images were obtained using a Hitachi SU8230 SEM instrument equipped with an Oxford Instruments Aztec Energy EDX system. Transmission electron microscopy (TEM) images were recorded on a JEOL TEM 4000EX instrument (JEOL, Japan) operating at 300 kV. FTIR was conducted with a Thermo Scientific Nicolet iS50 (USA) with an optical velocity of 0.6329 and a resolution of 4 cm⁻¹. Powder X-ray measurements were performed by using an X'Pert PRO Alpha-1 diffraction XRD system with Cu K α radiation to identify the crystalline phase of the composite. Nitrogen sorption–desorption isotherms have been collected using a Tristar porosimeter (Micromeritics, USA) to determine the surface area and pore size distribution of the samples. The alloy was polished with sandpapers to remove surface oxides for XRD measurements. ¹H NMR spectra were acquired on a Bruker Avance III 400 spectrometer in CD₃CN. Solid-state ¹³C cross-polarization (CP)-MAS NMR spectra were acquired using a Bruker Avance III-HD 300 MHz spectrometer. The sample was spun at 10 kHz using a 4 mm zirconia rotor at room temperature. The contact time for cross-polarization was set to 3 ms for both samples. A total of 1024 scans were collected with a delay of 4 and 8 s. The ¹³C chemical shifts were calibrated with respect to the adamantane observed at 38.45 ppm.

Structure Simulation. Structure discovery using the evolutionary algorithm. Crystal structures of $\text{Mg}(\text{OEt})_2$ and $\text{Mg}(\text{OH})(\text{OPr})$ at zero temperature and zero pressure were predicted using the Universal Structure Predictor: Evolutionary Xtallography (USPEX) code.^{28–30} In this computational scheme, the molecular crystal module was adopted, in which the OEt, OH, and OPr compounds are treated as rigid balls to avoid the internal decompositions. Moreover,

a population size of 40 structures was used in each generation and the enthalpy convergences of $\text{Mg}(\text{OEt})_2$ and $\text{Mg}(\text{OH})(\text{OPr})$ were reached after seven-generation runs. The enthalpy calculations involved were performed using the density functional theory (DFT), as implemented in the VASP package.^{31,32} The Perdew–Burke–Ernzerhof (PBE) exchange–correlation (XC) functional³³ and a plane-wave energy cutoff E_{cut} of 400 eV were adopted. Moreover, the Brillouin zone was sampled with a high resolution up to $2\pi \times 0.04 \text{ \AA}^{-1}$ and the vdW-TS method³⁴ was used to correct the vdW interactions in DFT calculations. In addition, in order to search the potential crystal structures of $\text{Mg}(\text{OEt})_2$ and $\text{Mg}(\text{OH})(\text{OPr})$, multiple runs with the conventional cell including 2, 4, and 8 formula units have been performed. The resulting most stable structure of $\text{Mg}(\text{OH})(\text{OPr})$ was further used to compute the vibrational density of states with the finite difference method implemented in the PHONOPY code,³⁵ comparing with the experimental IR spectrum.

■ ASSOCIATED CONTENT

SI Supporting Information

The Supporting Information is available free of charge at <https://pubs.acs.org/doi/10.1021/acsami.1c21757>.

EDS element mapping of $\text{Mg}_{0.8}\text{Li}_{0.2}$ and $\text{Mg}_{0.3}\text{Li}_{0.7}$ alloys, BET nitrogen adsorption–desorption isotherms of Mg ethoxides, TEM micrographs and TGA analysis of Mg ethoxide nanoparticles and Mg *n*-propoxide nanowires, and calculated FTIR pattern of Mg *n*-propoxide nanowires (PDF)

■ AUTHOR INFORMATION

Corresponding Author

Gleb Yushin – School of Materials Science & Engineering, Georgia Institute of Technology, Atlanta, Georgia 30332, United States; orcid.org/0000-0002-3274-9265; Email: yushin@gatech.edu

Authors

Shunrui Luo – School of Metallurgy and Environment, Central South University, Changsha 410083, PR China; School of Materials Science & Engineering, Georgia Institute of Technology, Atlanta, Georgia 30332, United States; orcid.org/0000-0003-4910-4604

Kostiantyn Turcheniuk – School of Materials Science & Engineering, Georgia Institute of Technology, Atlanta, Georgia 30332, United States

Lihua Chen – School of Materials Science & Engineering, Georgia Institute of Technology, Atlanta, Georgia 30332, United States; orcid.org/0000-0002-9852-8211

Ah-Young Song – School of Materials Science & Engineering, Georgia Institute of Technology, Atlanta, Georgia 30332, United States

Wenqiang Hu – School of Materials Science & Engineering, Georgia Institute of Technology, Atlanta, Georgia 30332, United States; orcid.org/0000-0002-9298-8663

Xiaolei Ren – School of Materials Science & Engineering, Georgia Institute of Technology, Atlanta, Georgia 30332, United States; College of Environment and Resources, Chongqing Technology and Business University, Chongqing 400067, PR China

Zifei Sun – School of Chemistry and Biochemistry, Georgia Institute of Technology, Atlanta, Georgia 30332, United States

Rampi Ramprasad – School of Materials Science & Engineering, Georgia Institute of Technology, Atlanta,

Georgia 30332, United States; orcid.org/0000-0003-4630-1565

Complete contact information is available at: <https://pubs.acs.org/doi/10.1021/acsami.1c21757>

Notes

The authors declare the following competing financial interest(s): G.Y. and Georgia Tech are stockholders of Sila Nanotechnologies, Inc.

■ ACKNOWLEDGMENTS

This work was mostly supported by Sila Nanotechnologies, Inc.

■ REFERENCES

- (1) Bradley, D.; Carter, D. Metal Oxide Alkoxide Polymers: Part I. The Hydrolysis Of Some Primary Alkoxides Of Zirconium. *Can. J. Chem.* **1961**, *39* (7), 1434–1443.
- (2) Young, K. *Mixed Metal Alkoxides as Ascatalyst Precursors*; Durham University: 1989.
- (3) Holloway, C. E.; Melnik, M. Magnesium Compounds: Classification and Analysis of Crystallographic and Structural Data. *J. Organomet. Chem.* **1994**, *465* (1), 1–63.
- (4) Arora, A. K.; Jaswal, V. S.; Singh, K.; Singh, R. Applications of Metal/Mixed Metal Oxides as Photocatalyst: (A Review). *Orient. J. Chem.* **2016**, *32* (4), 2035.
- (5) Turevskaya, E. P.; Yanovskaya, M. I.; Turova, N. Y. Preparation of Oxide Materials from Metal Alkoxides. *Inorg. Mater.* **2000**, *36* (3), 260–270.
- (6) Atanasov, S. E.; Kalanyan, B.; Parsons, G. N. Inherent Substrate-Dependent Growth Initiation and Selective-Area Atomic Layer Deposition of TiO_2 Using “Water-Free” Metal-Halide/Metal Alkoxide Reactants. *J. Vac. Sci. Technol. A* **2016**, *34* (1), No. 01A148.
- (7) Wang, X.; Yushin, G. Chemical Vapor Deposition and Atomic Layer Deposition for Advanced Lithium Ion Batteries and Supercapacitors. *Energy Environ. Sci.* **2015**, *8* (7), 1889–1904.
- (8) Lei, D.; Benson, J.; Magasinski, A.; Berdichevsky, G.; Yushin, G. Transformation of Bulk Alloys to Oxide Nanowires. *Science* **2017**, *355* (6322), 267–271.
- (9) Wang, F.; Turcheniuk, K.; Wang, B.; Song, A.-Y.; Ren, X.; Vallamattam, A.; Park, A.; Hanley, K.; Zhu, T.; Yushin, G. Mechanisms of Transformation of Bulk Aluminum–Lithium Alloys to Aluminum Metal–Organic Nanowires. *J. Am. Chem. Soc.* **2018**, *140* (39), 12493–12500.
- (10) Luo, S.; Turcheniuk, K.; Song, A.-Y.; Narla, A.; Kim, D.; Magasinsky, A.; Yushin, G. Conversion of Mg–Li Bimetallic Alloys to Magnesium Alkoxide and Magnesium Oxide Ceramic Nanowires. *Angew. Chem., Int. Ed.* **2020**, *59* (1), 403–408.
- (11) Huo, D.; Kim, M. J.; Lyu, Z.; Shi, Y.; Wiley, B. J.; Xia, Y. One-Dimensional Metal Nanostructures: From Colloidal Syntheses to Applications. *Chem. Rev.* **2019**, *119* (15), 8972–9073.
- (12) Zhu, C.; Peng, H.-C.; Zeng, J.; Liu, J.; Gu, Z.; Xia, Y. Facile Synthesis of Gold Wavy Nanowires and Investigation of Their Growth Mechanism. *J. Am. Chem. Soc.* **2012**, *134* (50), 20234–20237.
- (13) Nikoobakht, B.; El-Sayed, M. A. Preparation and Growth Mechanism of Gold Nanorods (NRs) Using Seed-Mediated Growth Method. *Chem. Mater.* **2003**, *15* (10), 1957–1962.
- (14) Li, P.; Zhan, H.; Tian, S.; Wang, J.; Wang, X.; Zhu, Z.; Dai, J.; Dai, Y.; Wang, Z.; Zhang, C.; Huang, X.; Huang, W. Sequential Ligand Exchange of Coordination Polymers Hybridized with In Situ Grown and Aligned Au Nanowires for Rapid and Selective Gas Sensing. *ACS Appl. Mater. Interfaces* **2019**, *11* (14), 13624–13631.
- (15) Bole, L. J.; Judge, N. R.; Hevia, E. Untangling the Complexity of Mixed Lithium/Magnesium Alkyl/Alkoxy Combinations Utilised in Bromine/Magnesium Exchange Reactions. *Angew. Chem., Int. Ed.* **2021**, *60* (14), 7626–7631.

(16) Petrus, R.; Sobota, P. Magnesium and Zinc Alkoxides and Aryloxides Supported by Commercially Available Ligands as Promoters of Chemical Transformations of Lactic Acid Derivatives to Industrially Important Fine Chemicals. *Coord. Chem. Rev.* **2019**, *396*, 72–88.

(17) Keyzer, E. N.; Lee, J.; Liu, Z.; Bond, A. D.; Wright, D. S.; Grey, C. P. A General Synthetic Methodology to Access Magnesium Aluminate Electrolyte Systems for Mg Batteries. *J. Mater. Chem. A* **2019**, *7* (6), 2677–2685.

(18) Jiang, F.; Feng, G.; Xu, C.; Qing, S.; Wu, Q.; Yu, Y.; Zhang, Q.; Jiang, W. Novel Facile Nonhydrolytic Sol-Gel Synthesis of MgAl_2O_4 Nanocrystal From Bimetallic Alkoxides. *J. Sol-Gel Sci. Technol.* **2021**, *100* (3), 555–561.

(19) Thoms, H.; Epple, M.; Viebrock, H.; Reller, A. Magnesium Alcoholates as Precursors for Magnesia. *J. Mater. Chem.* **1995**, *5* (4), 589–594.

(20) Mishra, S.; Daniele, S. Molecular Engineering of Metal Alkoxides for Solution Phase Synthesis of High-Tech Metal Oxide Nanomaterials. *Chem.—Eur. J.* **2020**, *26* (42), 9292–9303.

(21) Muga, C. O.; Zhang, Z. W. Strengthening Mechanisms of Magnesium-Lithium Based Alloys and Composites. *Adv. Mater. Sci. Eng.* **2016**, *2016*, 1078187.

(22) Guglielmi, M.; Carturan, G. Precursors for Sol-Gel Preparations. *J. Non-Cryst. Solids* **1988**, *100* (1), 16–30.

(23) Lutz, H. Zur Kenntnis der Erdalkalimethylate. IR-Spektroskopische Und Röntgenographische Untersuchungen an $\text{Mg}(\text{OCH}_3)_2$, $\text{Ca}(\text{OCH}_3)_2$, $\text{Sr}(\text{OCH}_3)_2$ und $\text{Ba}(\text{OCH}_3)_2$. *Anorg. Allg. Chem.* **1967**, *353* (3–4), 207–215.

(24) Thoms, H.; Epple, M.; Reller, A. The Thermal Decomposition of Magnesium Alcoholates To Magnesia (MgO): Studies by IR and Thermal Analysis. *Solid State Ionics* **1997**, *101-103*, 79–84.

(25) Turova, N. Y. Metal Oxoalkoxides. Synthesis, Properties and Structures. *Russ. Chem. Rev.* **2004**, *73* (11), 1041–1064.

(26) Starikova, Z. A.; Yanovsky, A. I.; Turevskaya, E. P.; Turova, N. Y. The Structure of the Crystal Solvate of Magnesium Methoxide with Methanol, $\text{Mg}(\text{OMe})_2 \cdot 3.5\text{MeOH}$. *Polyhedron* **1997**, *16* (6), 967–974.

(27) Bradley, D. C. Metal Alkoxides. *Metal-Organic Compounds*; American Chemical Society: 1959; Vol. 23, pp 10–36.

(28) Lyakhov, A. O.; Oganov, A. R.; Valle, M. Crystal Structure Prediction Using Evolutionary Approach. *Modern Methods of Crystal Structure Prediction*; John Wiley & Sons: 2011; pp 147–180.

(29) Oganov, A. R.; Glass, C. W. Crystal Structure Prediction Using Ab-Initio Evolutionary Techniques: Principles and Applications. *J. Chem. Phys.* **2006**, *124* (24), 244704.

(30) Zhu, Q.; Oganov, A. R.; Glass, C. W.; Stokes, H. T. Constrained Evolutionary Algorithm for Structure Prediction of Molecular Crystals: Methodology and Applications. *Acta Crystallogr., Sect. B: Struct. Sci.* **2012**, *68* (3), 215–226.

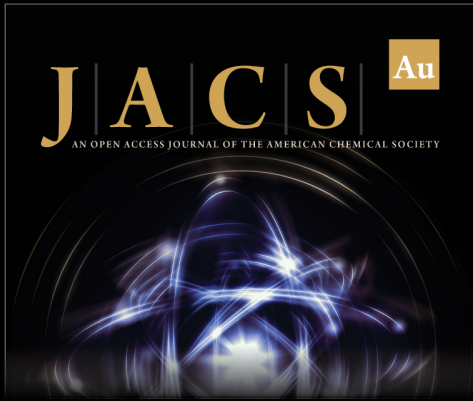
(31) Kresse, G.; Furthmüller, J. Efficient Iterative Schemes for Ab-Initio Total-Energy Calculations Using a Plane-Wave Basis Set. *Phys. Rev. B* **1996**, *54* (16), 11169.

(32) Kresse, G.; Furthmüller, J. Efficiency of Ab-Initio Total Energy Calculations for Metals and Semiconductors Using a Plane-Wave Basis Set. *Comput. Mater. Sci.* **1996**, *6* (1), 15–50.

(33) Perdew, J. P.; Burke, K.; Ernzerhof, M. Generalized Gradient Approximation Made Simple. *Phys. Rev. Lett.* **1996**, *77* (18), 3865.

(34) Tkatchenko, A.; Scheffler, M. Accurate Molecular Van Der Waals Interactions from Ground-State Electron Density and Free-Atom Reference Data. *Phys. Rev. Lett.* **2009**, *102* (7), No. 073005.

(35) Togo, A.; Tanaka, I. First Principles Phonon Calculations in Materials Science. *Scr. Mater.* **2015**, *108*, 1–5.



JACS Au
AN OPEN ACCESS JOURNAL OF THE AMERICAN CHEMICAL SOCIETY

Editor-in-Chief
Prof. Christopher W. Jones
Georgia Institute of Technology, USA

Open for Submissions 

pubs.acs.org/jacsau  ACS Publications
Most Trusted. Most Cited. Most Read.